Quasielastic π^--nucleus scattering at 950 MeV/c

Y. Fujii,[1,*] O. Hashimoto,[1] T. Nakagawa,[1] Y. Sato,[1] T. Takahashi,[1] J. T. Brack,[2] C. J. Gelderloos,[2] M. V. Keilman,[2] R. J. Peterson,[2] M. Itoh,[3] H. Sakaguchi,[3] H. Takeda,[3] K. Aoki,[4] H. Hotchi,[4] H. Noumi,[4] Y. Ohta,[4] H. Outa,[4] M. Sekimoto,[4] M. Youn,[4] S. Ajimura,[5] T. Kishimoto,[5] H. Bhang,[6] H. Park,[6] and R. Sawafta[7]

[1]*Department of Physics, Tohoku University, Sendai 980-8578, Japan*

[2]*Nuclear Physics Laboratory, University of Colorado, Boulder, Colorado 80309-0446*

[3]*Department of Physics, Kyoto University, Kyoto 606-8502, Japan*

[4]*High Energy Accelerator Research Organization (KEK), Ibaraki 305-0801, Japan*

[5]*Department of Physics, Osaka University, Osaka 560-0043, Japan*

[6]*Department of Physics, Seoul National University, Seoul 151-742, Korea*

[7]*Physics Department, North Carolina A & T State University, Greensboro, North Carolina 27411*

(Received 14 May 1999; revised manuscript received 31 May 2000; published 22 August 2001)

Quasielastic scattering cross sections have been measured with a 950 MeV/c π^- beam on targets of ^{2}H, ^{6}Li, C, Ca, Zr, and ^{208}Pb, over a range of three-momentum transfers from 350 through 650 MeV/c. Results for carbon are compared to a finite-nucleus continuum random-phase approximation calculation including distortions. The pion spectra at our lowest range of momentum transfers show less scalar/isoscalar correlation than predicted.

DOI: 10.1103/PhysRevC.64.034608 PACS number(s): 25.80.Ls

I. INTRODUCTION

Quasielastic scattering is a process in which an incident particle elastically and incoherently interacts with only one nucleon inside a nucleus, with all the other nucleons being spectators. At intermediate energies this process dominates the nuclear response, showing two characteristic features: one is that the position of the peak corresponds to that of elastic scattering by a free nucleon, and the other is that the width of the peak reflects internal motion of individual nucleons in the target nucleus. Nuclear correlations can be studied with this process, by measuring the distribution of the quasielastic strength [1]. Quasielastic scattering of electrons has been extensively studied using their short wavelengths, deep penetration, and well-known couplings to nucleons. However, the coupling of electrons to nucleons is almost entirely electromagnetic, and hadronic probes are needed to explore the full set of spin and isospin couplings. A recent example is the study of isovector spin-transverse and spin-longitudinal quasielastic scattering with the polarized (p,n) reaction [2,3].

Mesonic probes can be used to study other couplings than reached by lepton and baryon beams. Quasielastic noncharge exchange (NCX) scattering by pion and K^+ beams occurs largely through scalar-isoscalar couplings, while pion single-charge exchange (SCX) acts through an isovector, largely scalar, coupling. Both (π,π') (NCX) [4] and $(\pi^\pm,\pi^0)$ (SCX) [5] reactions were measured using pions of 624 MeV/c at LAMPF. The quasielastic peak positions for the $(\pi^\pm,\pi^0)$ reaction showed shifts toward higher energy loss than for free $\pi^- p$ scattering below about $q = 400$ MeV/c, while no shifts were observed for the (π,π') reaction. This difference was tentatively explained as arising from the difference in effective particle-hole interactions for different channels. These studies demonstrated that pion quasielastic scattering can be used to study nuclear responses in the scalar-isoscalar and scalar-isovector channels. At large momentum transfers, however, the outgoing pions from those studies have such low energies as to be likely to interact again to form the prominent Δ resonance. A higher pion beam energy is needed to avoid this complication and to maintain a long mean free path within the nuclear medium. The $(K^+,K^{+\prime})$ quasielastic reaction at 705 MeV/c [6] was measured at the Alternating Gradient Synchrotron (AGS) at Brookhaven National Laboratory, taking advantage of the small K^+N cross sections to give a long mean free path within nuclei to reach high densities of nucleons. Theoretical calculations compared to these data were performed in a finite-nucleus continuum random-phase approximation (RPA) framework [7]. The calculation described the experimental results well and provided a constraint on the strength of the effective particle-hole interaction in the scalar-isoscalar channel. The model used in that calculation is also applied below to the present data.

The present experiment is a study of quasielastic π^--nucleus scattering at 950 MeV/c, principally to investigate the nuclear response using a scalar-isoscalar dominant probe. An advantage of the present experiment at 950 MeV/c compared to the previous one at 624 MeV/c is the greater predominance of the scalar-isoscalar channel. The momentum transfer dependence of the spin/isospin content of pion-nucleon scattering cross section at the beam momentum of 950 MeV/c is shown in Fig. 1. The $\pi^- N$ cross sections in the four allowed spin/isospin channels are taken from the SM95 solution to SAID [8], assuming charge symmetry. The fraction of the scalar-isoscalar channel is more than 55% and up to 75% over a momentum transfer range from 350 to 550 MeV/c, which our spectra will emphasize.

II. EXPERIMENT AND DATA ANALYSIS

The experiment was performed at the 12 GeV proton synchrotron of the High Energy Accelerator Research Organiza-

*Electronic address: fujii@lambda.phys.tohoku.ac.jp

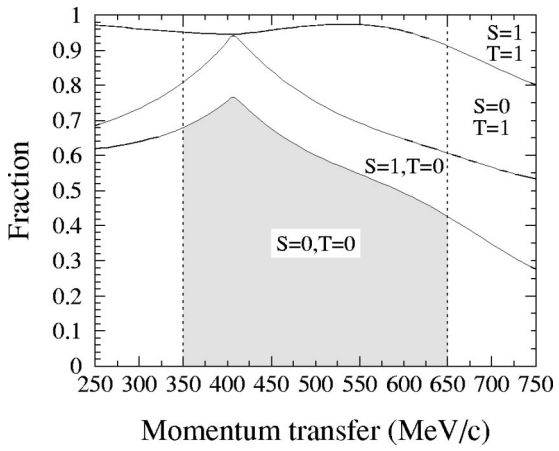

FIG. 1. The q dependence of the spin/isospin content of the pion-nucleon scattering cross section at a beam momentum of 950 MeV/c. The present experiment covers the range from 350 through 650 MeV/c. As elsewhere in this work, q is measured in the laboratory frame.

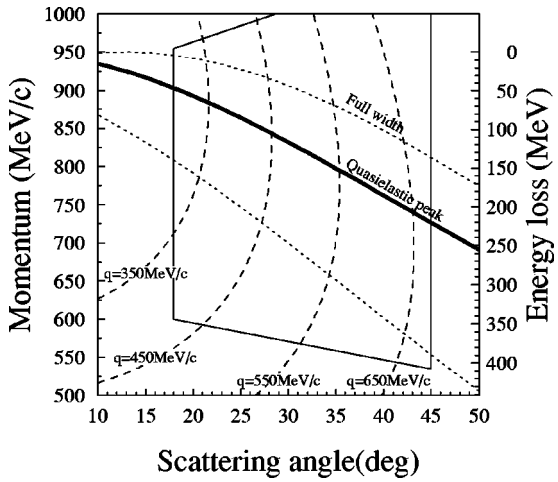

FIG. 2. Kinematics of the present experiment. The thin solid line shows the region where measurements were made. The q-fixed loci are shown in the dashed lines. The thick solid line shows kinematics of a quasielastic peak and the dotted lines show full width of a quasielastic peak calculated with a Fermi-gas model ($k_F = 221$ MeV/c).

tion (KEK) [9]. A negative-pion beam was delivered to the target by the K6 beam line, which was equipped with a DC separator. The beam momentum was analyzed by a beam line spectrometer, which comprises a QQDQQ magnet system, three arrays of scintillator hodoscopes, and four sets of drift chambers capable of tracking high-rate beam particles. The momentum spread of the beam was $\pm 1.2\%$. The typical beam intensity at the experimental target was 1.1×10^6 particles/spill, where the beam duration was 1.8 s and the spill repetition cycle was 4 s. The beam size (rms) was typically 6.3 mm horizontal and 13.0 mm vertical.

Scattered pions were analyzed with the Superconducting Kaon Spectrometer (SKS) [9]. It consists of a 11 MJ superconducting dipole magnet, four sets of drift chambers, arrays of time-of-flight (TOF) scintillators, Aerogel Čerenkov counters, and Lucite Čerenkov counters. The SKS was positioned at a fixed laboratory scattering angle of 30°. Since the SKS has a large solid angle of 100 msr, it could cover an angular range of $\pm 15°$. The momentum acceptance of the spectrometer was $\pm 20\%$. Four magnetic field settings (860, 780, 720, and 630 MeV/c central momentum) were used to cover the entire quasielastic region, allowing good overlap regions. The present setup covers momentum transfers from 350 to 650 MeV/c and energy loss up to 350 MeV, as shown in Fig. 2.

A veto plastic scintillator (24 cm wide) was placed along the beam direction 40 cm downstream from the scattering targets, subtending $\pm 17°$. This was used to reject the large background from the pion beam not interacting with the scattering target but directly hitting a detector frame downstream. The veto counter cut into the most forward events accepted by the SKS, so only pion scattering angles beyond 20° were analyzed. Comparing continuum spectra with and without the veto at the same low beam rate, the difference was less than 3% across the quasielastic region. We conclude that use of this veto system did not affect the shape or magnitude of our quasielastic spectra beyond 20°.

Natural isotopic targets of CH_2 (3.5 g/cm^2), C (4.6 g/cm^2), Ca (3.1 g/cm^2), and Zr (3.4 g/cm^2) and highly isotopically enriched targets of C^2H_2 (1.4 g/cm^2), $^6Li^2H$ (2.0 g/cm^2), and ^{208}Pb (4.6 g/cm^2) were irradiated in the present experiment. The size of the targets was 4.6 cm wide and 4.1 cm high for the lead target and 10 cm wide and 10 cm high for the other targets, more than 3 times as large as the beam size. The targets were chosen to study the A dependence of the quasielastic scattering over a wide range of nuclear sizes. The deuteron target was used to ensure that we correctly account for scattering on both neutrons and protons.

Free $\pi^- p$ scattering cross sections were measured with the CH_2 and C targets at several beam momenta. The differential cross sections were derived using an SKS acceptance function determined by a Monte Carlo simulation, in which measured field maps, geometry and efficiencies of detectors, and the beam profile measured during the experiment were used. Figure 3 shows an example of the mapped acceptance and the loci of elastic proton events at several beam momenta. These cross sections were compared to those from SAID [8] as shown in Fig. 4 and normalized to the SAID cross sections. The normalization factor was 1.05. The overall accuracy of this normalization was 5% for the quasielastic region, as determined by the comparison between the shapes of the measured and the SAID cross sections. In addition, the elastic scattering cross sections for carbon at 900 MeV/c are in agreement with those of Takahashi *et al.* at 895 MeV/c [10] within 15%. The systematic error of the cross sections was estimated to be 11%, determined by the above agreement with SAID, the accuracy with which overlapping spectra agreed (never worse than 7%), and the effects of the veto counter. We include no uncertainty for the $\pi^- p$ cross sections of SAID, since any theoretical comparisons to our data are likely to use these same cross sections.

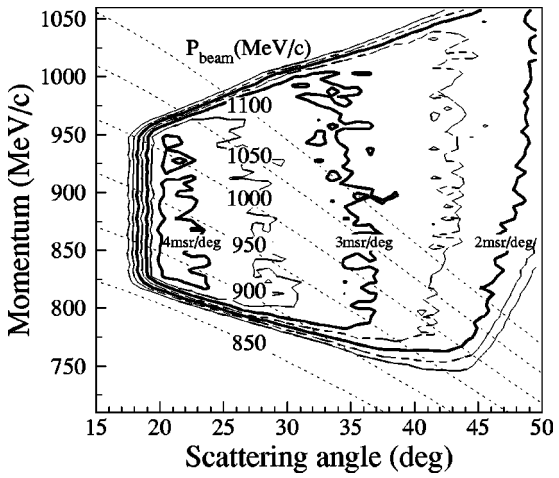

FIG. 3. Effective solid angle of the SKS for the highest SKS field setting (860 MeV/c central momentum), covering most of the quasielastic spectra as determined by ray tracing through the measured field profile. The loci of elastic proton events at several beam momenta used for checks of the normalization are shown as dotted lines.

The energy resolution was 3.0 MeV [full width at half maximum (FWHM)], as determined by the carbon elastic peak. This is good enough for quasielastic scattering studies. Events were collected into momentum transfer bins of full width 25 MeV/c or about 1.8°, which was wider than the angular resolution of 0.8°, to get enough statistical accuracy events at a range of angles and outgoing energies.

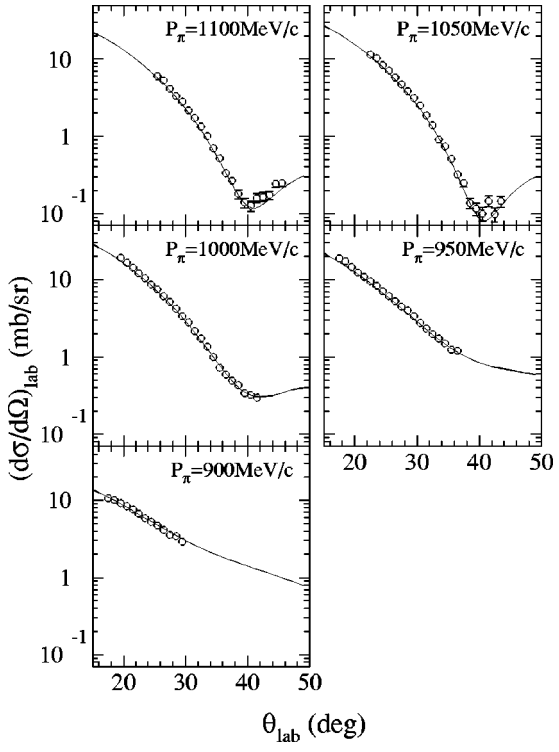

FIG. 4. Differential cross sections for $\pi^- p$ elastic scattering measured with the highest SKS field setting. The open circles show the cross sections before normalization to the SAID cross sections. The solid lines show the results of SAID.

Doubly differential cross sections for ^{2}H, ^{6}Li, C, Ca, Zr, and ^{208}Pb are presented as a function of energy loss ω for a given momentum transfer bin, where ω was defined as the difference between the initial and final laboratory kinetic energies of the scattered pions. Deuteron spectra were extracted by subtracting the C spectra from C^2H_2 spectra after normalization. The ^{6}Li spectra were similarly obtained from ^{6}Li^{2}H and deuteron spectra.

III. RESULTS

A. Doubly differential cross sections

Figure 5 shows the doubly differential cross sections for ^{2}H, C, and ^{208}Pb at fixed q of 350, 500, and 650 MeV/c. The measured spectra clearly show the characteristic shape of a quasielastic peak, centered near the energy loss corresponding to that of free $\pi^- N$ elastic scattering (125 MeV at $q=500$ MeV/c) and broadened due to the internal motion of individual nucleons inside the nucleus. These features are familiar from electron scattering continuum spectra, which, however, require an awkward radiative unfolding procedure not required in the pion scattering.

The observed spectra were fitted by a sum of three components: a quasielastic peak, a background, and additional Gaussian peak(s) for elastic and inelastic scattering. For the nuclei other than the deuteron, an asymmetric Gaussian with exponential cutoff factor $C(\omega)$ was used to describe each quasielastic peak as follows:

$$f_{\rm qe}(\omega)=\begin{cases} c_1 C(\omega)\exp\left[-\frac{1}{2}\left(\frac{\omega-c_2}{c_3}\right)^2\right] & \text{if} \quad \omega\leqslant c_2, \\ c_1 C(\omega)\exp\left[-\frac{1}{2}\left(\frac{\omega-c_2}{c_4}\right)^2\right] & \text{if} \quad \omega> c_2, \end{cases} \tag{1}$$

$$C(\omega)=\begin{cases} 0 & \text{if} \quad \omega\leqslant\omega_{\rm el}, \\ 1-\exp\left(-\frac{\omega-\omega_{\rm el}}{c_5}\right) & \text{if} \quad \omega>\omega_{\rm el}, \end{cases} \tag{2}$$

$$\omega_{\rm el}=\sqrt{q^2+M_{\rm tgt}^2}-M_{\rm tgt}, \tag{3}$$

where $\omega_{\rm el}$ is the energy loss due to target recoil and $M_{\rm tgt}$ is a target mass. This formalism was introduced by Erell *et al.* [11]. The cutoff factor, $C(\omega)$, describes the suppression due to Pauli blocking. In addition, in the case of fitting calcium spectra, an additional Gaussian was included to describe a contribution from a small hydrogen contamination. The width and central energy of the additional Gaussian were fixed to those of the $\pi^- p$ scattering data.

For the deuteron spectra, a shifted Lorentzian distribution was used to describe each quasielastic peak:

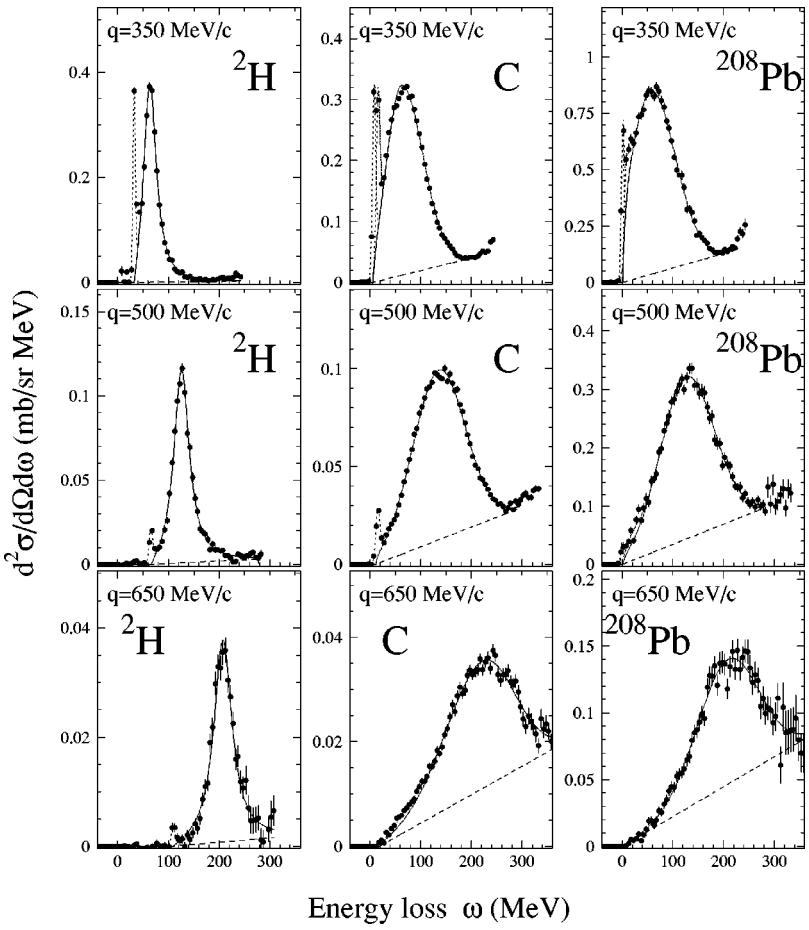

FIG. 5. Doubly differential cross sections for ^{2}H, C, and ^{208}Pb at fixed q of 350, 500, and 650 MeV/c. The error bars show statistical uncertainties only. The lines show the fitted quasielastic peak (solid), contribution from nonquasielastic process (dashed), and peak(s) for elastic and inelastic scattering (dotted).

$$f_{\rm qe}(\omega)=\begin{cases} 0 & \\ \quad \text{if } \omega\leqslant\omega_{\rm el}, & \\ c_1\left[\dfrac{1}{(\omega-\omega_{\rm el}-c_2)^2+c_3}-\dfrac{1}{(\omega-\omega_{\rm el}+c_2)^2+c_3}\right] & \\ \quad \text{if } \omega>\omega_{\rm el}. & \end{cases} \tag{4}$$

The original form (without $\omega_{\rm el}$) was introduced by Esbensen and Bertsch [12] to parametrize a free response of a semi-infinite slab model.

There will also be contributions to the strength under the quasielastic peak from nonquasielastic processes: multiple scattering [7], two-particle–two-hole ($2p$-$2h$) excitations [13], and pion production [14], for example. In the present analysis, these contributions were subtracted as ''background,'' assuming the shape as a linear function of ω,

$$f_{\rm bg}(\omega)=\begin{cases} 0 & \text{if} \quad \omega\leqslant\omega_{\rm el}, \\ c_0(\omega-\omega_{\rm el}) & \text{if} \quad \omega>\omega_{\rm el}. \end{cases} \tag{5}$$

Each of the spectra in Fig. 5 shows examples of the fitting. The spectra were well fitted by the present fitting functions. Then, cross sections and the centroids and widths of the quasielastic peaks were deduced. The quasielastic cross sections for calcium were deduced from the extracted cross sections, which include a small correction from an oxygen contaminant, assuming from the observed H peak some contaminant of $Ca(OH)_2$.

The model uncertainty of the fits due to the ''background'' assumption was estimated by also ascribing the ''background'' only to Δ production. A Breit-Wigner peak at the energy loss corresponding to Δ production was assumed and folded with the quasielastic peak shape in the fitting. For the carbon data at $q=500$ MeV/c, this procedure gives changes of $+15\%$ to the quasielastic cross section, $+6\%$ to the width, and $+2$ MeV to the centroid. These changes can be taken to represent a systematic uncertainty in the effects of the continuous background under the quasielastic peak. At the largest q of 650 MeV/c, these changes increase to $+40\%$, $+10\%$, and $+5$ MeV, respectively. Error bars from Figs. 6 to 9 include all the systematic errors.

B. Quasielastic cross sections

Figure 6 shows the extracted quasielastic cross sections for π^--nucleus scattering as a function of momentum transfer. The solid lines show fitted results to a noninteracting Fermi-gas model,

$$\frac{d\sigma}{d\Omega}=A_{\rm eff}B(q,k_F)\left(\frac{d\sigma}{d\Omega}\right)_{\pi N}, \tag{6}$$

with a parameter $A_{\rm eff}$. $B(q,k_F)$ is the Pauli blocking factor

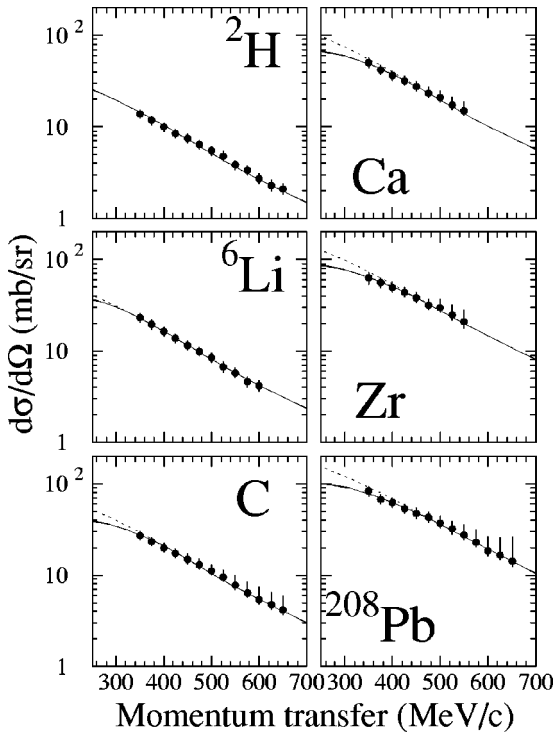

FIG. 6. Integrated quasielastic cross sections for ^{2}H, ^{6}Li, C, Ca, Zr, and ^{208}Pb as a function of momentum transfer. The solid lines show fits to the cross sections, using average free scattering cross sections and a scale factor $A_{\rm eff}$, and the dotted lines show the same fits without the Pauli blocking factor.

[15], and k_F is the Fermi momentum of the target nucleus. The dotted lines show the fits without the Pauli blocking factor. The factor $A_{\rm eff}$ can be interpreted as the effective number of nucleons participating in the quasielastic scattering. Since effects of Pauli blocking are small for the measured kinematical region, k_F is fixed to the experimental values of the (e,e') data of Ref. [16] for this figure. Better results will follow below. $(d\sigma/d\Omega)_{\pi N}$ is the elementary $\pi^- N$ elastic scattering cross section at 950 MeV/c, averaged over all nucleons in the nucleus. We use the free $\pi^- N$ cross sections, even for scattering within nuclei. A recent calculation of meson properties in nuclei suggests little change of the π mass and little change of a σ meson mass that carries the scalar-isoscalar interaction favored by our experiment [17]. It therefore seems appropriate to use free $\pi^- N$ scattering amplitudes that were obtained with the phase shift code SAID [8] in the present analysis. The present analysis reproduces the q dependence of $d\sigma/d\Omega$ with the single parameter $A_{\rm eff}$ as shown in Fig. 6, showing the validity of the factorization of the quasielastic cross sections as given in Eq. (6).

C. Effective number of nucleons

The fitted values of $A_{\rm eff}$ from Fig. 6 are listed in Table I. $A_{\rm eff}$ is expected to follow a power law of atomic mass A,

$$A_{\rm eff}^{\rm exp} = N_0 A^{\alpha}, \tag{7}$$

as shown in Fig. 7 and as is also known for other quasielastic meson scattering [4,6,18]. The best fit value for the exponent

TABLE I. Extracted values for the effective nucleon numbers $A_{\rm eff}$, Fermi momenta k_F, and peak shifts relative to free scattering $\Delta\omega_0$ (at $q=500$ MeV/c). $A_{\rm eff}$ and k_F were obtained from fits to cross sections and widths at all q's.

Target	A	$A_{\rm eff}$	k_F (MeV/c)	$\Delta\omega_0(q=500$ MeV/c) (MeV)
^{2}H	2.0	$1.76^{+0.08}_{-0.03}$	$53.4^{+1.1}_{-1.1}$	2.5 ± 2.5
^{6}Li	6.0	$2.77^{+0.10}_{-0.10}$	$146.6^{+6.2}_{-5.4}$	3.3 ± 3.0
C	12.0	$3.57^{+0.19}_{-0.08}$	$183.4^{+9.9}_{-3.8}$	11.7 ± 2.7
Ca	40.1	$6.75^{+0.40}_{-0.20}$	$198.7^{+8.0}_{-5.3}$	7.5 ± 2.7
Zr	91.2	$9.21^{+0.57}_{-0.31}$	$214.3^{+12.5}_{-10.8}$	4.6 ± 3.2
^{208}Pb	208.0	$11.70^{+0.72}_{-0.29}$	$192.5^{+14.3}_{-8.4}$	1.6 ± 3.0

α is 0.42 ± 0.01, smaller than the exponent of 0.56 ± 0.03 found for π^- NCX scattering at 624 MeV/c [4]. The exponent $\alpha<1$ indicates a shadowing of nucleons in the nucleus by neighboring nucleons. For electron scattering, α is near unity because of the weakness of electron-nucleon interaction. The present value of 0.42 indicates that pions are largely absorbed at the nuclear surface and thus scattered only from the surface region of a nucleus.

The value of $A_{\rm eff}$ can be estimated by using an eikonal approximation based on Glauber theory [18]:

$$A_{\rm eff}^{\rm calc} = \int d^2b\, T(b) e^{-\sigma_T T(b)}, \tag{8}$$

$$T(b) = \int_{-\infty}^{+\infty} dz \rho(\sqrt{b^2+z^2}), \tag{9}$$

where $\rho(r)$ is the proton density taken from the ground state charge distributions of Ref. [19]. The neutron density distribution is assumed to be the same as that of protons. σ_T is the total $\pi^- N$ cross section, averaged over all nucleons in the nucleus using values for $\pi^- p$ (53.77 mb) and $\pi^- n$ (23.75 mb) scattering at 950 MeV/c [8]. The open circles in Fig. 7 show the results of the calculation. The slope of the A dependence is well reproduced, though the calculated $A_{\rm eff}$ are smaller than the experimental observations. The larger ex-

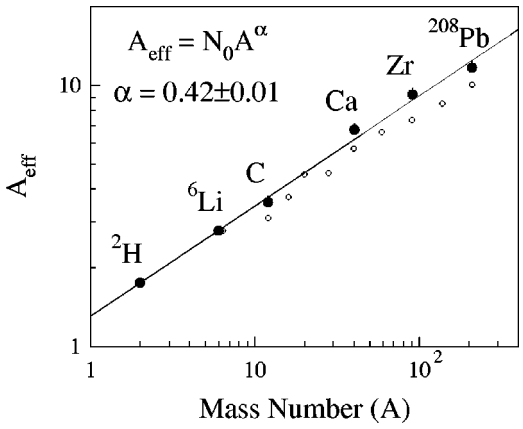

FIG. 7. Fit of the effective number of nucleons to a power law. The open circles are the results of an eikonal calculation.

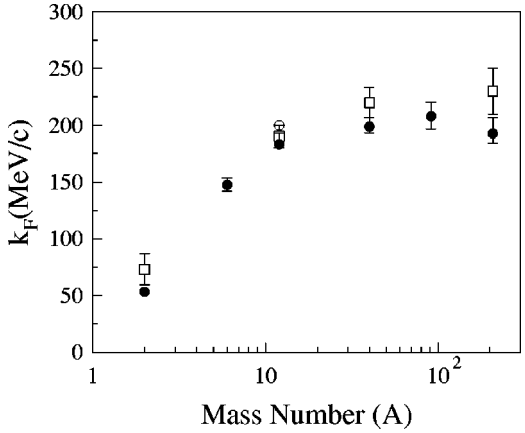

FIG. 8. Fermi momenta extracted from measured widths of the quasielastic peaks are compared. The solid circles are the present results and the open squares are the values from the $(K^+,K^{+\prime})$ reaction [6]. The open circle for carbon is at a beam momentum of 624 MeV/c [4].

perimental $A_{\rm eff}$ may be due to a change of the $\pi^- N$ total cross section in the nuclear medium. It is noted that this difference is present regardless of the assumed ''background'' shape, since the systematic uncertainties from the alternative treatment of this subtraction are all positive.

D. Peak width

In the simple relativistic Fermi-gas model the width (FWHM) of the quasielastic peak is determined by the Fermi momentum k_F of the struck nucleons:

$$\Gamma_{\rm FG}=\frac{1}{\sqrt{2}}[\sqrt{M^{*2}+(q+k_F)^2}-\sqrt{M^{*2}+(q-k_F)^2}], \tag{10}$$

where M^* is the effective mass of the struck nucleon, here taken to be the free mass of a nucleon. The Fermi momentum for each target nucleus was thus derived using Eq. (10) from the experimental widths obtained by fitting the quasielastic peak. For the present spectra the reduced χ^2 values ranged from 0.4 to 1.7. These Fermi momenta are summarized in Table I and shown as the solid circles in Fig. 8. They are compared to results obtained from K^+ scattering [6] (the open squares). The K^+ penetrates more deeply into nuclei where the nuclear density and thus local Fermi momentum is higher, resulting in a wider quasielastic peak. The Fermi momentum previously extracted from the π^--C quasielastic scattering at $P_\pi=624$ MeV/c (the open circle) is very similar with the present observation [4]. Equation (10) was applied to the deuteron data so that the data can be included in the figure as a reference, although the Fermi-gas model is not appropriate.

E. Peak position

The peak positions of the quasielastic scattering process in a nuclear target would be shifted from that of the free

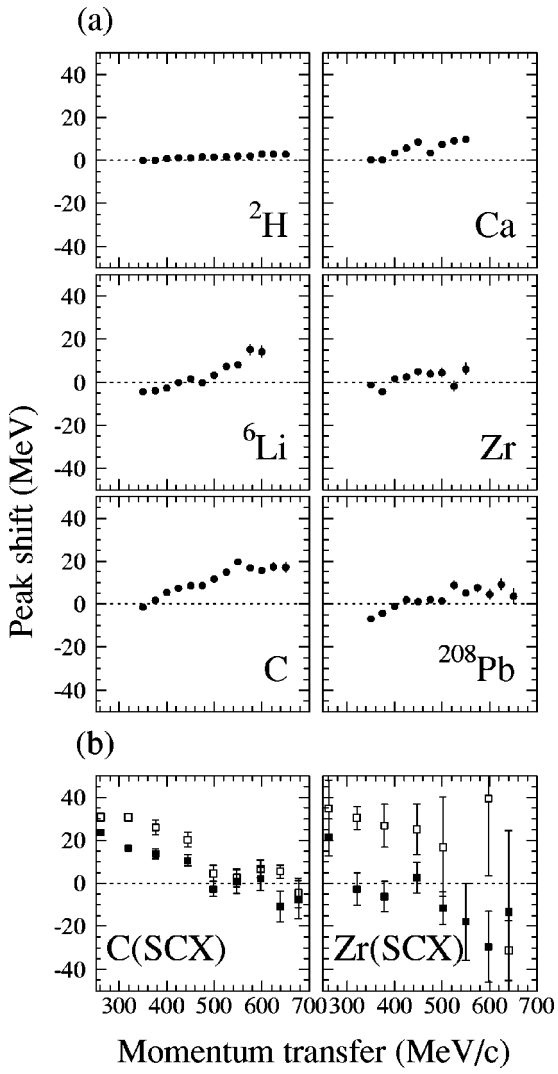

FIG. 9. Quasielastic peak shifts relative to scattering from hydrogen for (a) the present result, and (b) π^- (solid squares) and π^+ (open squares) SCX at 624 MeV/c [5].

space scattering due to the interaction of the struck nucleon with its mean field or with its neighbor nucleons. In Fig. 9(a) we show the energy loss shift of the peak positions of the quasielastic scattering on the nuclear target relative to that of hydrogen. The shift is positive for a quasielastic peak with greater energy loss relative to the free kinematics. In Fig. 9(b) we also show shifts for the quasielastic SCX of negative-pion (the solid squares) and positive-pion (the open squares) beams at 624 MeV/c [5] for comparison with the present mostly scalar-isoscalar quasielastic scattering. These are to be averaged to cancel the Coulomb effect. The striking difference of the q dependence between mostly scalar-isoscalar and scalar-isovector probes can be explained from the interactions presented in Ref. [20].

In the previous (π,π') NCX experiment at 624 MeV/c [4] no significant peak shift was observed for momentum transfers up to about 600 MeV/c. However, those results are not inconsistent with the present data due to large uncertainties of the previous data.

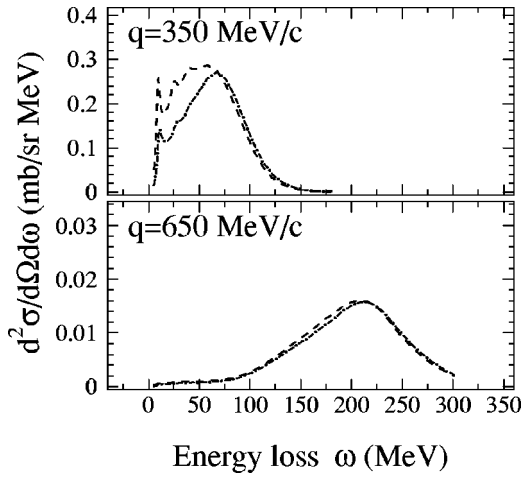

FIG. 10. Computed cross sections for π^--^{12}C quasielastic scattering without interactions (dashed-dot lines) and in the RPA in the scalar-isoscalar channel only (dashed lines).

F. Comparison with a theoretical calculation

Doubly differential cross sections for carbon are compared with a theoretical calculation based on a finite-nucleus continuum RPA framework using a density-dependent particle-hole interaction [21]. This model does not use the factorized form of Eq. (6), but takes into account distortions of pions by means of a Glauber-type calculation. The same framework was successfully applied to other reactions with strongly interacting beams, (p,n) [22] and (K,K') [7].

Figure 10 shows a comparison between a free (dashed-dot lines) response and RPA (dashed lines) response in the scalar-isoscalar channel for π^--^{12}C quasielastic scattering. As seen in the figure, there is little difference between these calculations at $q=650$ MeV/c, but the nuclear scalar-isoscalar interactions have an important effect at 350 MeV/c. Figure 11 shows π^--^{12}C quasielastic cross sections compared with the RPA calculations. The open circles show the quasielastic portion of the experimental data; the linear background determined by the fitting described in Sec. III A has been subtracted from the experimental data. The solid lines show the cross section with full interaction, while the dashed (dotted) lines represent the cross sections through the scalar-isoscalar (non-scalar-isoscalar) channel. The RPA responses shift toward higher energy loss with higher q, which is consistent with the present data. The origin of the positive shift of the RPA responses depends on q. For $q=350$ and 450 MeV/c, the shift is due to a q dependence of the scalar-isoscalar response. However, at $q=550$ and 650 MeV/c it is due to an increasing contribution from non-scalar-isoscalar responses. The q dependence of the observed peak shift on the carbon target is qualitatively reproduced by the RPA calculation, except for the lowest q of 350 MeV/c. At the larger q, the agreement between the RPA spectra and the experimental spectra would imply that interactions in scalar-isoscalar and the other channels are appropriately taken into account in the calculation. At low-energy losses for $q=350$ MeV/c, the interacting RPA overestimates the present data even though the interaction strength has been already set to half of its expected value, as needed for similar

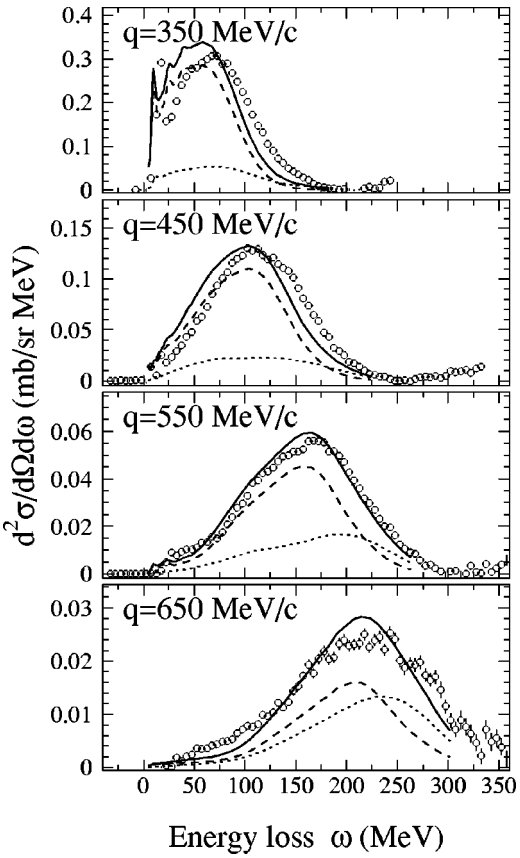

FIG. 11. π^--^{12}C quasielastic cross sections compared with the RPA calculation. The open circles show the quasielastic portion of the experimental data. The solid lines show the RPA cross section with all channels. The dashed lines show the RPA cross section only with the scalar-isoscalar channel, and the dotted lines show the contributions from non-scalar-isoscalar channels.

RPA calculations in Ref. [7] to reproduce the K^+ quasielastic data. The present data would agree best with an RPA prediction with very small or no scalar-isoscalar nuclear interaction.

IV. CONCLUSIONS

We have measured quasielastic and continuum scattering of 950 MeV/c π^- on nuclei ranging from ^{2}H through ^{208}Pb. The measurement was done with single fixed spectrometer angle taking advantage of the large solid angle of the SKS spectrometer, with which good angular and energy resolution were also realized. The overall normalization of the measured spectra was confirmed by comparing the cross section of $\pi^- p$ elastic scattering with those of the SAID calculation.

The present experiment offered high-quality quasielastic spectra for laboratory three-momentum transfers from 350 through 650 MeV/c. Since radiative corrections are not needed for pion beams in contrast to electron beams, these spectra are simple and clean even for ^{208}Pb; those data are very similar in quality and shape to those for carbon.

We have summarized our observations by fitting the spectra above a background and obtained singly differential cross sections, and centroids and widths of the quasielastic peaks.

The integrated cross sections follow a power law in A, as observed for other meson quasielastic reactions, and are nearly as predicted by a simple Glauber model. Peak widths were used to extract Fermi momenta, which approach saturation as nuclear densities saturate for heavy targets. Our Fermi momenta are lower than those found for K^+ scattering, as expected since pions interact at lower nuclear densities. The energy shifts of the quasielastic maxima follow the general trend expected from the momentum dependence of NN interactions, in a direction opposite to that found for SCX quasielastic spectra sensing only isovector NN interactions.

At the lowest q of 350 MeV/c, the present data are sensitive to scalar-isoscalar residual interactions, as included in the recent RPA calculations [7] to which we compare the data. Calculations of quasielastic K^+ scattering based on this model found a need to make those interactions weaker than expected. The present higher-quality π^- spectra show a further need to reduce collectivity than is provided by the RPA calculation. At larger q, the other spin/isospin channels become as important as the scalar-isoscalar channel. The good agreement with the present spectra would indicate that no relative change in those interactions is needed within the carbon nucleus.

ACKNOWLEDGMENTS

The authors would like to thank Dr. A. De Pace for allowing us to use the spectra of the RPA calculation. The support by the KEK-PS staff for the running of this experiment is greatly appreciated. Dr. R. Chrien kindly loaned us the ^{6}Li^{2}H sample.

[1] W.M. Alberico, M. Ericson, and A. Molinari, Nucl. Phys. **A379**, 429 (1982).
[2] L.B. Rees, J.M. Moss, T.A. Carey, K.W. Jones, J.B. McClelland, N. Tanaka, A.D. Bacher, and H. Esbensen, Phys. Rev. C **34**, 627 (1986).
[3] T.N. Taddeucci *et al.*, Phys. Rev. Lett. **73**, 3516 (1994).
[4] J.E. Wise *et al.*, Phys. Rev. C **48**, 1840 (1993).
[5] R.J. Peterson, S. Høibråten, J. Ouyang, M.R. Braunstein, X.Y. Chen, M.D. Kohler, B.J. Kriss, D.J. Mercer, D.S. Oakley, and D.L. Prout, Phys. Lett. B **297**, 238 (1992).
[6] C.M. Kormanyos *et al.*, Phys. Rev. C **51**, 669 (1995).
[7] A. De Pace, C. García-Recio, and E. Oset, Phys. Rev. C **55**, 1394 (1997).
[8] R.A. Arndt, I.I. Strakovsky, R.L. Workman, and M.M. Pavan, Phys. Rev. C **52**, 2120 (1995).
[9] T. Fukuda *et al.*, Nucl. Instrum. Methods Phys. Res. A **361**, 485 (1995).
[10] T. Takahashi *et al.*, Phys. Rev. C **51**, 2542 (1995).
[11] A. Erell, J. Alster, J. Lichtenstadt, M.A. Moinester, J.D. Bowman, M.D. Cooper, F. Irom, H.S. Matis, E. Piasetzky, and U. Sennhauser, Phys. Rev. C **34**, 1822 (1986).
[12] H. Esbensen and G.F. Bertsch, Ann. Phys. (N.Y.) **157**, 255 (1984).
[13] W.M. Alberico, A. Molinari, A. De Pace, M. Ericson, and Mikkel B. Johnson, Phys. Rev. C **34**, 977 (1986).
[14] J.D. Zumbro *et al.*, Phys. Rev. Lett. **71**, 1796 (1993).
[15] G.F. Bertsch and O. Scholten, Phys. Rev. C **25**, 804 (1982).
[16] R.R. Whitney, I. Sick, J.R. Ficenec, R.D. Kephart, and W.P. Trower, Phys. Rev. C **9**, 2230 (1974).
[17] A.M. Rakhimov, F.C. Khanna, U.T. Yakhshiev, and M.M. Musakhanov, Nucl. Phys. **A643**, 383 (1998).
[18] J. Ouyang, S. Høibråten, and R.J. Peterson, Phys. Rev. C **47**, 2809 (1993).
[19] H. de Vries, C.W. de Jager, and C. de Vries, At. Data Nucl. Data Tables **36**, 495 (1987).
[20] T. Shigehara, K. Shimizu, and A. Arima, Nucl. Phys. **A492**, 388 (1989).
[21] A. De Pace (private communication).
[22] A. De Pace and M. Viviani, Phys. Rev. C **48**, 2931 (1993).